PAPER

Check for updates

Synthesis and characterization of silver–thiolate dynamic crosslinking waterborne polyurethane with room-temperature self-healing properties†

Mengyun Zhang,[ab] Shanjun Ding,[a] Riming Cong[a] and Yunjun Luo ![ORCID] *[a]

Waterborne polyurethanes (WPUs), commonly used as coatings and adhesives, produce microcracks when suffering from severe environmental stimuli or continuous mechanical loads. So far, there have only been limited self-healing functional groups, such as disulfide bonds, or Diels−Alder reactions, utilized in WPUs. Herein, we have prepared a novel self-healing waterborne polyurethane (SHWPU) by introducing silver−thiol coordination interactions, which exhibit excellent self-healing performance. WPU−Ag@S-0.50 with microcracks could recover to its original state at room temperature within 30 min. The self-healing efficiency in terms of its tensile strength is 98.69%, demonstrating that introducing silver−thiol coordination interactions is an effective strategy to realize self-healing.

1. Introduction

Recently, self-healing waterborne polyurethanes (SHWPUs) have been developed rapidly, and different SHWPUs have sprung up. Most SHWPUs are based on the chemical modification methods of introducing disulfide bonds or Diels–Alder reactions to the structures of WPUs. However, self-healing materials are not only limited to these two methods. Self-healing materials can be divided into two categories: external and intrinsic self-healing materials. External materials include microcapsules,[1] microfibers,[2,3] and microvascular networks.[4] Intrinsic materials are fabricated by hydrogen bonds,[5] disulfide bonds,[6–8] Diels–Alder reactions,[9–13] metallophilic attractions,[14–19] *trans*-esterification reactions,[20,21] *etc.* Although disulfide bonds and Diels–Alder reactions are the most widely used methods for self-healing, it is still of great significance to explore new methods for synthesizing SHWPUs.

Metallophilic attraction is a kind of interaction that is intermediate between chemical bonds and supramolecular interactions. Self-healing materials prepared by this interaction possess a particular advantage compared with those involving covalent bonds, that is, they achieve the self-healing target more quickly. The silver–thiol interaction is one kind of metallophilic attraction. Some studies have reported silver–thiolate

coordination polymers showing intriguing self-healing performance. Odriozola *et al.*[16] used thiol-functionalized silicone oil to crosslink silver nanoparticles (Ag NPs) to obtain a mechanically consistent elastomer. This material could recover completely within 24 hours at room temperature, indicating that it possesses good self-healing ability. Agarwal *et al.*[22] synthesized a thiol-terminated poly(*cis*-1,4-isoprene) (PIP) material. They coordinated it with silver trifluoroacetate to form a dynamically crosslinked thermoplastic elastomer as the silver–thiol coordination interactions endow the polymer with the unique self-healing performance and exceptional value in medical science. Dupin *et al.*[23] prepared a kind of injectable and self-healing dynamic hydrogel based on Au/Ag–thiolate/disulfide interactions. Based on the exchange reactions between thiol and silver, this hydrogel could substitute the synovial fluid in the joints of the human body, demonstrating that it possesses great value in medical fields, such as rheumatoid arthritis (RA) and intervertebral disc (IVD).

Introducing silver–thiol coordination bonds to WPUs is a significant technical challenge. To prepare dynamically crosslinked SHWPUs, the strategies that can be adopted are as follows: (1) preparing thiol-terminated WPUs followed by adding Ag NPs; (2) *in situ* reducing Ag NPs on WPUs followed by the addition of multi-functional thiols. We choose the second strategy, as much effort has been devoted to the synthesis of WPUs grafted with Ag NPs. To produce Ag NPs, the chemical reduction of silver ions from a silver salt is a widely used method because of its simplicity.[24] Reducing agents commonly used for silver ions are sodium citrate,[25] sodium borohydride,[26] hydrazine hydrate,[27] glucose,[28] ascorbic acid,[29] alcohol,[30] and DMF.[31,32] In some cases, the synthesis of WPUs grafted with Ag NP composites

[a] School of Materials Science and Engineering, Beijing Institute of Technology, Beijing 100081, P. R. China. E-mail: yjluo@bit.edu.cn

[b] Institute of Nuclear and New Energy Technology, Tsinghua University, 100084, Beijing, China

† Electronic supplementary information (ESI) available. See DOI: https://doi.org/10.1039/d2ma00300g

uses these reducing agents. Buragohain et al.[32] prepared a hyperbranched polyurethane modified by Ag NPs with the help of DMF. Lu et al.[26] utilized carboxylate-functionalized WPUs as a stabilizer to coordinate with AgNO₃. Then, Ag NPs were *in situ* obtained by reduction reactions with NaBH₄. Sun et al.[33] introduced PTMG as flexible segments to PUs and terminated them with hydroxyls, which functioned as *in situ* reduction sites to reduce AgNO₃ to Ag NPs. As these methods may introduce inorganic salt impurities or toxic organic solvents to WPUs, green and clean ways must be explored.[34,35]

This study uses H_2O_2 as the reducing agent to prepare WPUs grafted with Ag NP composites. As H_2O_2 will not introduce impurities to the WPU system, it is clean and environmentally friendly. At first, the main chains of WPUs were grafted with Ag NPs through the following steps: (1) AgNO₃ was coordinated with the partial carboxyl of WPUs; (2) AgNO₃ was decomposed at high temperatures to produce WPUs grafted with Ag_2O NPs; (3) H_2O_2 was used to reduce Ag_2O NPs at room temperature to produce WPUs grafted with Ag NPs. After that, a silver–thiol dynamic crosslinking network was formed by introducing the hydrophilic difunctional thiol 3,6-dioxa-1,8-octanedithiol into the WPU system grafted with Ag NPs. The structures of the samples were confirmed by XRD, XPS, TEM, and FTIR analyses, while their self-healing properties were probed by optical microscopy, tensile mechanics, and rheology. Finally, the self-healing mechanism was elucidated to provide a deeper understanding of self-healing materials.

2. Materials and methods

2.1. Materials

Polypropylene glycol (PPG-N210, industrial grade, Tianjing Petrochemical Co., Ltd, China) was dried at 120 °C for 4 h before use. Isophorone diisocyanate (IPDI, industrial grade, Bayer AG, Germany) was used as received. Silver nitrate (AgNO₃, analytical grade, pure, Shandong Xiya Chemical Co., Ltd, China) was protected from light and stored in a desiccator. 2-Bis(hydroxymethyl) propionic acid (DMPA, industrial grade, Beijing Linshi Fine Chemicals & New Materials Co., Ltd, China) was dried at 100 °C for 12 h. 3,6-Dioxa-1,8-octanedithiol (Analytical grade, pure, Aladdin) was used as received. Tetrahydrofuran (THF, analytical grade, pure, Beijing Chemical Works, China), triethylamine (TEA, analytical grade, Tianjing Fuchen Co., China), and 1,4-butylene glycol (BDO, analytical pure, Tianjing Fuchen Co., China) were dried with 4 Å molecular sieves. Hydrogen peroxide (H_2O_2, chemically pure, 30% aqueous solution, Tianjing Damao Chemical Factory, China) was used as received. DI water was prepared in our lab.

2.2. Instrumentation

The particle size and Zeta-ζ of the WPU–Ag emulsions were tested using a laser particle size analyzer (Malvern Zetasizer Nano ZS90). The WPU–Ag emulsions were diluted to 1 wt% using DI water, and every sample was tested three times. The viscosity was measured by a viscometer (Brookfield programmable DV-II+pro)

using a zero-size rotor with a frequency of 150 s⁻¹ and a temperature of 25 °C. The centrifugal stability was characterized using a high-speed centrifuge (ZONKIA, HC-3018). Equal amounts of emulsions were placed in two centrifuge tubes that were positioned symmetrically in the centrifuge. The speed was set to 3000 rpm, and the centrifugal force was 1.5 kg. After centrifuging for 5 min, no precipitation was observed, indicating that the emulsions were stable. XRD analyses were conducted using an X' Pert Pro MPD diffractometer with monochromatic Cu Kα radiation (λ = 1.54 Å), and XPS tests were carried out on a Thermo Fisher K-Alpha instrument. The WPU–AgNO₃, WPU–Ag₂O, and WPU–Ag samples were used to form films of size 10 mm × 10 mm × 6 mm. The infrared spectra were collected using a Nicolet 8700 FTIR (Thermo Nicolet Corporation) with a Ge ATR probe. The scan range was from 4000 to 400 cm⁻¹ with a resolution of 4 cm⁻¹ for a total of 48 times. The emulsion of WPU–Ag-1.00 was dissolved in ethanol and attached to a copper net to dry for transmission electron microscopy (TEM) experiments. Images were collected on a JEOL-2100 transmission electron microscope operated at 200 kV. The glass transition temperature Tg was determined by differential scanning calorimetry (DSC) using a Mettler Toledo DSC instrument. The temperature was increased from −80 to 150 °C under a nitrogen atmosphere at a heating rate of 10 °C min⁻¹. The cohesive behavior of microcracks on the WPU films was monitored using an optical microscope (DM 2500P, Leica) with a Linkam hot stage; the sizes of the samples were 10 mm × 10 mm × 0.6 mm. Microcracks was made using a micrometer scratch instrument,[36] and the depth of the microcracks was about 0.3 mm. Uniaxial tensile tests were carried out using a universal testing machine (Instron-6022, Shimadzu Co., Ltd) at a tensile rate of 100 mm min⁻¹. Rheological experiments were performed on an advanced modular rheometer (HAAKE MARs) using a pair of 20 mm parallel plates and disk-shaped samples. Frequency sweeps were conducted from 10⁻² to 10² rad s⁻¹ at 30 °C.

2.3. Synthesis of waterborne polyurethane grafted with Ag NPs (WPU–Ag)

In a typical procedure, PPG-N210, IPDI, and DMPA were added to a four-necked flask equipped with a mechanical stirrer, nitrogen inlets, and a condenser. The mixture was heated to 85 °C and reacted for 3 h. Then, the temperature was lowered to 70 °C, and BDO was added to the system and reacted for another 2 h to complete the chain extension reactions. Following this, a certain amount of THF was added to the mixture when the viscosity was high. After that, TEA was added to the mixture for 30 min at room temperature to partially neutralize the carboxyl groups of DMPA and form ionic pairs. The most critical step was the introduction of Ag NPs. Different contents of AgNO₃ were dissolved in 5 g DI water and poured into flasks to coordinate with the remaining carboxyl groups of DMPA for 3 h until the color of the mixture turned a homogeneous pale yellow. After reacting at 100 °C for 1 h, the products gradually became dark red or brown-black. Subsequently, the mixture was cooled down to room temperature. Then, 6.5 g 30% H_2O_2 was poured into the flask, and the reduction reaction was allowed to proceed for 1 h.

The products turned bright yellow and were emulsified with DI water at 2000 rpm for 30 min, and the solvent was rotatory evaporated to obtain the WPU–Ag emulsions. The detailed formulas are shown in Table S1 (ESI†).

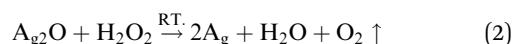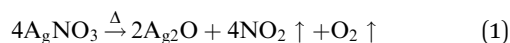## 2.4. Synthesis of silver–thiolate dynamically crosslinked waterborne polyurethane (WPU–Ag@S)

The WPU–Ag emulsion was blended quickly with hydrophilic 3,6-dioxa-1,8-octanedithiol in a 1:1 mole ratio of thiol to Ag. The mixture of WPU–Ag@S was then quickly poured into a PTFE mold at room temperature and dried for 7 days. Then, the mold was placed in a 40 °C oven for 24 h until the weight became constant. The final thickness of the film obtained was 0.6 mm, which was used for further tests. WPU–Ag@S samples with different contents of silver–thiol coordination bonds were prepared.

3. Results and discussion

### 3.1. Synthesis, structural characterization, and properties

This study adopted a facile *in situ* reduction method to synthesize WPU–Ag composites. Firstly, WPU prepolymers were obtained by polyaddition reactions of PPG-N210, IPDI, and DMPA. Then, they were extended using BDO to form WPU main chains. Following that, 75 wt% of the carboxyl groups of DMPA was neutralized by TEA. The remaining carboxyl groups were coordinated using different amounts of AgNO$_3$. Herein, DMPA not only plays a role in dispersing the WPUs well in water but also bridges the link between the WPUs and Ag NPs. After allowing sufficient time for coordination at room temperature, we obtained WPU–AgNO$_3$. Then, the following two steps of reduction were carried out based on the theory explained below:

$$4A_gNO_3 \xrightarrow{\Delta} 2A_{g2}O + 4NO_2 \uparrow + O_2 \uparrow \qquad (1)$$

$$A_{g2}O + H_2O_2 \xrightarrow{RT.} 2A_g + H_2O + O_2 \uparrow \qquad (2)$$

As shown by eqn (1), AgNO$_3$ decomposed on the WPUs into Ag$_2$O, NO$_2$, and O$_2$ at 100 °C, where Ag$_2$O aggregated into nanoparticles buried in the WPUs and NO$_2$ and O$_2$ were released into the air. As shown in eqn (2), the Ag$_2$O NPs in the WPUs were reduced by H$_2$O$_2$ to form a WPU–Ag composite, the O$_2$ produced was released into the air and H$_2$O was left in the system. After emulsification and rotatory evaporation, we obtained the WPU–Ag composite emulsions. There were no impurities and toxic solvents introduced into the system, demonstrating that this is a simple, economical, and environmentally friendly method for preparing emulsions of WPU–Ag. The detailed synthetic steps are listed in Scheme 1(a), and the structure of WPU–Ag is shown in Scheme 1(b). As thiols can coordinate with Ag NPs to form coordination bonds, the hydrophilic difunctional thiol 3,6-dioxa-1,8-octanedithiol was added to the WPU–Ag emulsion to create a dynamic cross-linking network, whose structure is shown in Fig. 1(c).

After synthesis, the emulsion properties were measured, and the results are listed in Table 1. As can be seen in Table 1, the mean particle sizes of WPU–Ag are smaller than that of the WPUs. This was because the Ag NPs were distributed on the surface of the WPU particles, decreasing the interaction between the ionic pairs and water. Therefore, the particle sizes of WPU–Ag are smaller. Abbas *et al.*[37] also found a similar phenomenon. They proposed that Ag NPs reduced the interchain interactions and molecular packing and even facilitated the migration of the carboxylate groups on the particle surfaces,
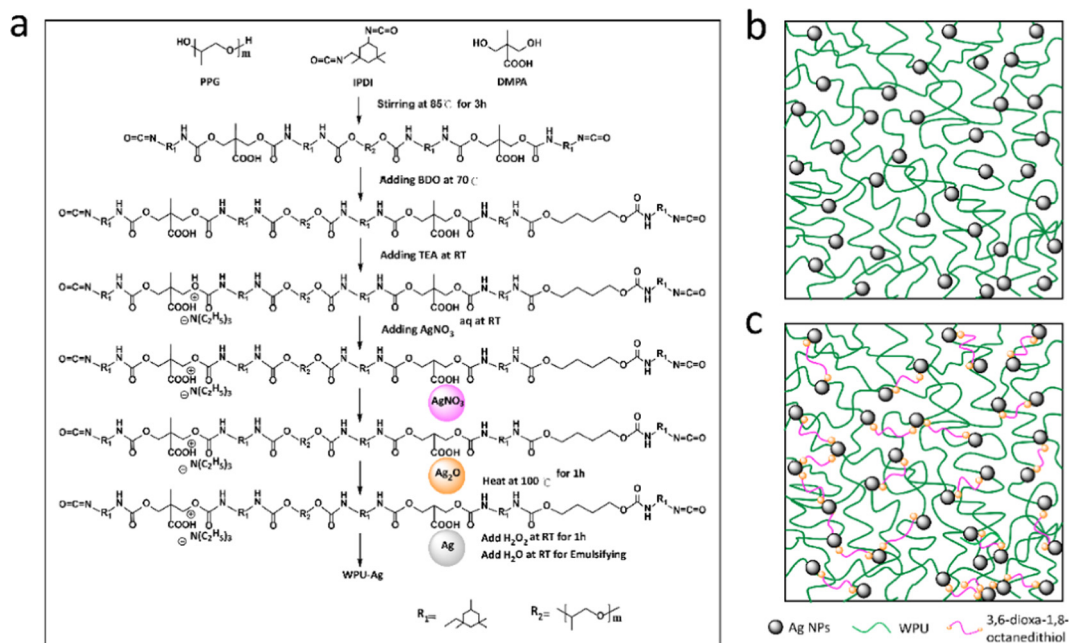
Scheme 1 (a) Synthetic steps of WPU–Ag, (b) the structure of WPU–Ag, and (c) the structure of WPU–Ag@S.
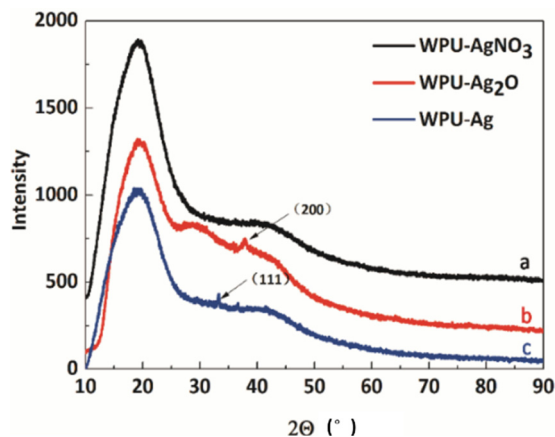
Fig. 1 XRD spectra of (a) WPU–AgNO₃, (b) WPU–Ag₂O and (c) WPU–Ag.

Table 1 Basic properties of the WPU–Ag emulsions

Samples	Mean particle size/nm	PDI	Zeta-ζ/mV	Viscosity/ mPa s	Centrifugal stability
WPU–Ag-0.00	128.9	0.097	−42.6	32.1	Stable
WPU–Ag-0.25	82.9	0.124	−31.5	44.4	Stable
WPU–Ag-0.50	97.6	0.090	−43.8	42.8	Stable
WPU–Ag-0.75	106.1	0.132	−39.9	31.4	Stable
WPU–Ag-1.00	114.0	0.157	−40.1	30.0	Stable

ultimately reducing the particle sizes. Except for WPU–Ag-0.00, the mean particle sizes of all the WPU–Ag composites increased with the silver content as the amount of Ag NPs distributed on each WPU particle increased, further leading to larger particle sizes. Moreover, all the PDIs are small, demonstrating that the emulsion droplets are uniform. The viscosity was also characterized, which is mainly influenced by the degree of ionization and particle size. As the ionization was basically constant, the

particle sizes increased with increasing content of Ag NPs, weakening the interactions between the particles and water and causing the viscosity to decrease. Another critical parameter for emulsions is their stability. The absolute values of Zeta-ζ of all the emulsions are much higher than 30 mV, showing that the emulsions are stable. The stability was also verified by centrifugation experiments. There were no precipitates observed at the bottom of centrifuge tubes, confirming that the emulsions were stable for more than 6 months. In fact, the emulsions could be stably stored for at least 8 months.

To confirm if the Ag NPs were introduced into the WPU system, XRD, the most direct characterization method, was employed. Here, the crystal structures of WPU–AgNO₃, WPU–Ag₂O, and WPU–Ag were characterized by XRD. The test results are shown in Fig. 1. In all the XRD curves, a prominent, broad diffraction peak at around 19.2° and a small broad diffraction peak at approximately 41.7° appear, indicating that samples have low crystallinity. This was due to the fact that the WPU chains were scattered with regular inter-planar spacing.[38,39] Fig. 1(a) presents the spectrum for WPU–AgNO₃. It shows identical broad diffraction peaks, as the ionic nature of AgNO₃ did not disrupt the microstructure of the WPUs. When WPU–AgNO₃ was heated to 100 °C, it began to decompose and aggregate into Ag₂O NPs, due to which a small crystalline peak appears at 37.9° in the spectrum in Fig. 1(b), corresponding to the (200) plane of Ag₂O NPs. As shown in Fig. 1(c), a small crystalline peak for WPU–Ag appears at 33.3°, which corresponds to the (111) plane of Ag NPs. The peaks for crystallinity were not prominent because the amount of silver source used was low. However, their signal peaks were still visible. Therefore, we preliminarily judged that we had obtained the WPU–Ag composite.

Additionally, TEM is also an effective way to characterize the structure of nanoparticles through morphological observation. As seen in Fig. 2(a), Ag₂O NPs are clustered and distributed on
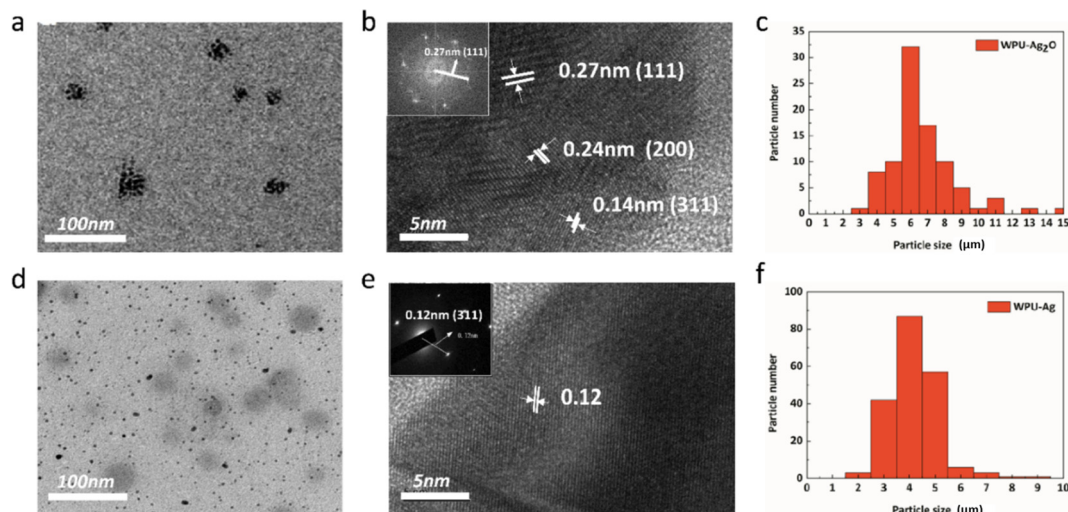

Fig. 2 (a) TEM image of WPU–Ag₂O; (b) HRTEM image of Ag₂O nanoparticles (inset is the selected area electron diffraction pattern of the Ag₂O nanoparticles); (c) particle size distribution of the Ag₂O NPs; (d) TEM image of WPU–Ag; (e) HRTEM image of Ag nanoparticles (inset is the selected area electron diffraction pattern of the Ag nanoparticles); and (f) particle size distribution of the Ag NPs.

the substrate. The magnified Ag_2O NPs are exhibited in Fig. 2(b). Their lattice spacings can be seen and measured. The lattice spacings of the (111), (200), and (311) planes are 0.27 nm, 0.24 nm, and 0.14 nm, respectively. The inset in Fig. 2(b) shows the selected area electron diffraction (SAED) pattern of the (111) plane, whose distance is 0.27 nm, in accordance with the measurement result, demonstrating that the particles are indeed Ag_2O NPs. The particle size distribution is shown in Fig. 2(c), and the mean particle size of the Ag_2O NPs is about 6.16 nm. These nanoparticles were reduced by H_2O_2, and their morphologies are shown in Fig. 2(d). The magnified Ag NPs are exhibited in Fig. 2(e). The lattice spacing of the (311) plane is 0.12 nm, which is consistent with the SAED pattern in the inset of Fig. 2(e), indicating that WPUs grafted with Ag NPs were synthesized successfully. Moreover, the mean particle size of Ag NPs calculated from the particle size distribution shown in Fig. 2(f), which is about 3.37 nm and less than the mean particle size of Ag_2O NPs, further evidence that the reduction process occurred.

As we have successfully synthesized the WPUs grafted with Ag NPs, silver–thiolate dynamic crosslinking waterborne polyurethane could be prepared by blending WPU–Ag and 3,6-dioxa-1,8-octanedithiol, where the mole ratio between Ag and dithiol is 2 : 1. Fig. 3 presents the FTIR spectra of WPU–Ag and WPU–Ag@S. As shown in Fig. 3(a), the peaks at 3357 cm^{-1}, 2936 cm^{-1}, 1707 cm^{-1} and 1095 cm^{-1} are attributed to the >NH, –CH3/>CH2, >C=O and –C–O–C– groups, respectively. As shown in Fig. 3(b), the peaks at 3319 cm^{-1}, 2915 cm^{-1}, 1714 cm^{-1} and 1111 cm^{-1} are attributed to the >NH, –CH3/>CH2, >C=O and –C–O–C– groups, respectively. These peaks are unique signals for WPUs. After the introduction of thiol, the characteristic peak of >NH shifted from 3357 cm^{-1} to 3319 cm^{-1}, indicating that more >NH groups formed hydrogen bonds, and the characteristic peak of >C=O shifted from 1707 cm^{-1} to 1714 cm^{-1}, indicating that fewer >C=O groups formed hydrogen bonds. These results indicate that more Ag NPs formed coordination bonds with thiols. In general, the FTIR peaks of Ag–thiol and Ag–carbonyl coordinating interactions appear at low wavenumbers below 400 cm^{-1}, which are not

observed in our FTIR spectra. To understand the bonding situations of Ag–thiol and Ag–carbonyl in the WPUs, we performed FTIR peak fitting on the carbonyl groups of WPU–Ag and WPU–Ag@S. The details are listed in the ESI.† The Ag–thiol coordination interactions were further explored through XPS and rheology tests.

Furthermore, the XPS test results for WPU–$AgNO_3$, WPU–Ag_2O, WPU–Ag, and WPU–Ag@S are shown in Fig. 4. Fig. 4(a) presents the wide scan surveys of the above four products, wherein the peaks at 284.8 eV, 399.8 eV, and 532.3 eV are attributed to the signals of C 1s, O 1s and N 1s, respectively. As can be seen clearly, the signals for Ag 3d in WPU–Ag were significantly higher than those of the other three samples, demonstrating that the Ag_2O NPs were completely reduced by H_2O_2. Fig. 4(b) presents the Ag 3d spectra. The peaks for Ag $3d_{5/2}$ and Ag $3d_{3/2}$ of WPU–$AgNO_3$ appear at 368.6 eV and 374.6 eV, respectively. The peaks for Ag $3d_{5/2}$ and Ag $3d_{3/2}$ of WPU–Ag_2O appear at 367.9 eV and 373.9 eV, respectively. The peaks for Ag $3d_{5/2}$ and Ag $3d_{3/2}$ of WPU–Ag appear at 368.2 eV and 374.2 eV, while those of WPU–Ag@S appear at 368.1 eV and 374.1 eV, respectively. The fitting curves coincide well with the original curves, demonstrating that the products obtained are pure. The percentages of Ag in WPU–$AgNO_3$, WPU–Ag_2O, and WPU–Ag are listed in Table S2 (ESI†).

DSC was used to test the glass transition temperatures of the WPUs. In general, there exist two glass transition temperatures in the DSC curves of the WPUs, denoted as T_{g1} and T_{g2}. As shown in Fig. 5(a), a wide temperature transition zone appears in the range of −18.4 °C to −3.7 °C, corresponding to T_{g1}. As T_{g1} is obviously lower than 0 °C, the soft segments of WPU–Ag could move at room temperature. Meanwhile, a small second glass transition temperature T_{g2} for the WPU–Ag series is observed at 79.6 °C to 96.5 °C, higher than room temperature, demonstrating that the movements of the hard segments of the WPUs are limited. ΔT_g is the difference between T_{g1} and T_{g2}. It reflects the microphase separation degree. The ΔT_g of WPU–Ag-0.50 is the smallest, demonstrating that its microphase separation degree is the smallest, and its phase mixing degree is the largest.
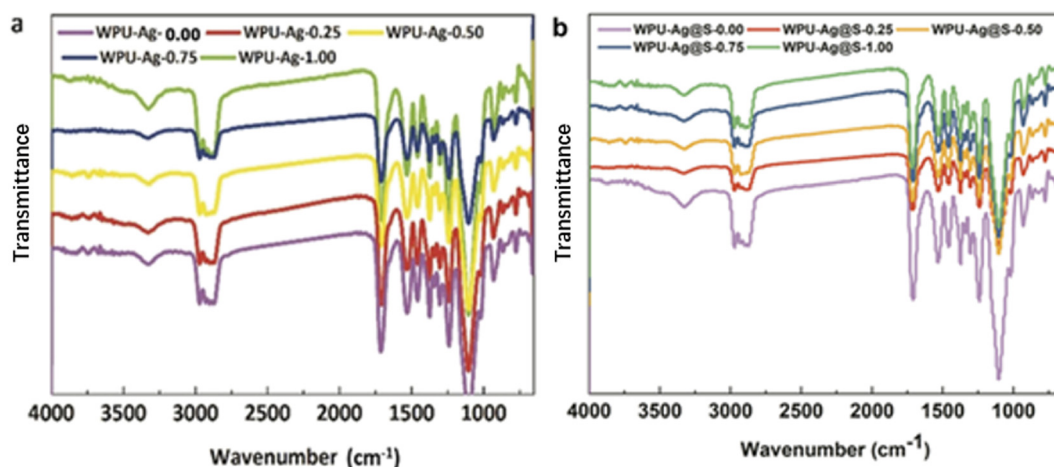

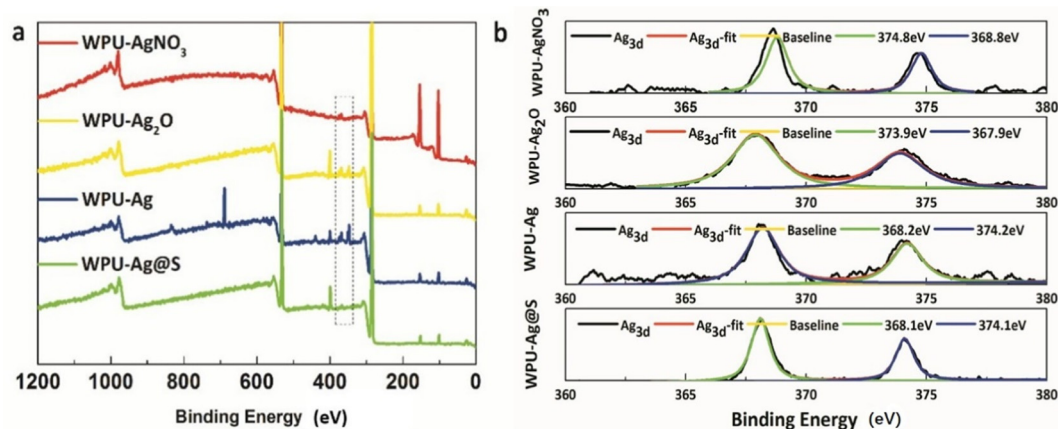**Fig. 3** FTIR spectra of the films of (a) the WPU–Ag series and (b) WPU–Ag@S series.

Fig. 4 (a) Survey spectra and (b) Ag 3d core-level spectra for WPU–AgNO$_3$, WPU–Ag$_2$O, WPU–Ag, and WPU–Ag@S.
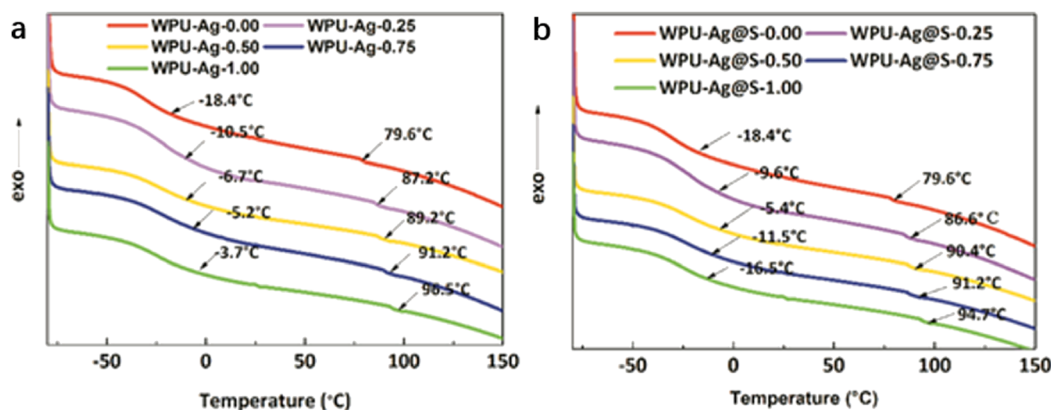

Fig. 5 DSC curves and glass transition temperatures T_{g1} and T_{g2} for the (a) WPU–Ag and (b) WPU–Ag@S series.

Similarly, as shown in Fig. 5(b), T_{g1} varies with the silver–thiol coordination interaction and shows a maximum value at −5.4 °C for WPU–Ag@S-0.50. Meanwhile, T_{g2} increases with the silver–thiol coordination interaction, and WPU–Ag@S-1.00 has the maximum T_{g2} of 94.7 °C. However, ΔT_g is the smallest at 95.8 °C for WPU–Ag@S-0.50, indicating the lowest microphase separation degree. This further proves that the molecular chains of WPU–Ag@S-0.50 diffuse and move more quickly. The detailed data are shown in Table 2.

Table 2 Glass transition temperatures for the WPU–Ag and WPU–Ag@S series

Samples	T_{g1} (°C)	T_{g2} (°C)	ΔT_g (°C)
WPU–Ag-0.00	−18.4	79.6	98.0
WPU–Ag-0.25	−10.5	87.2	97.7
WPU–Ag-0.50	−6.7	89.2	95.9
WPU–Ag-0.75	−5.2	91.2	96.4
WPU-Ag-1.00	−3.7	96.5	100.2
WPU–Ag@S-0.00	−18.4	79.6	98.0
WPU–Ag@S-0.25	−9.6	86.6	96.2
WPU–Ag@S-0.50	−5.4	90.4	95.8
WPU–Ag@S-0.75	−11.5	91.2	102.7
WPU–Ag@S-1.00	−16.5	94.7	111.2

3.2. Self-healing properties

The self-healing process of microcracks on the WPU–Ag@S films was observed under an optical microscope at room temperature, and the results are shown in Fig. 6. As seen in Fig. 6, the self-healing process can be divided into two kinds based on the variances of the –Ag@S– coordination bonds. In the first type, the two faces of the microcrack underwent approach, wetting, diffusion, and dynamic exchange reactions of the –Ag@S– coordination bonds, with random movements of the molecular chains when the content of silver (Ag/–COOH$_{remain}$) was less than the mole ratio of 0.50. In the second type, the microcrack matrix experienced plastic flow, which filled the valley of the microcrack, followed by dynamic exchange reactions of the –Ag@S– coordination bonds and random movements of the molecular chains when the content of silver (Ag/–COOH$_{remain}$) was more than the mole ratio of 0.50. As the variable parameters are the content of Ag NPs and hydrophilic 3,6-dioxa-1,8-octanedithiol, the material matrix becomes stiffer with an increase in Ag NPs and softer with the rise in 3,6-dioxa-1,8-octanedithiol. When the mole ratio of Ag and thiol is less than 0.5, the stiffness plays a significant role. When the mole ratio of Ag and thiol is more than 0.5, the softness plays an important role. Due to the synergy of
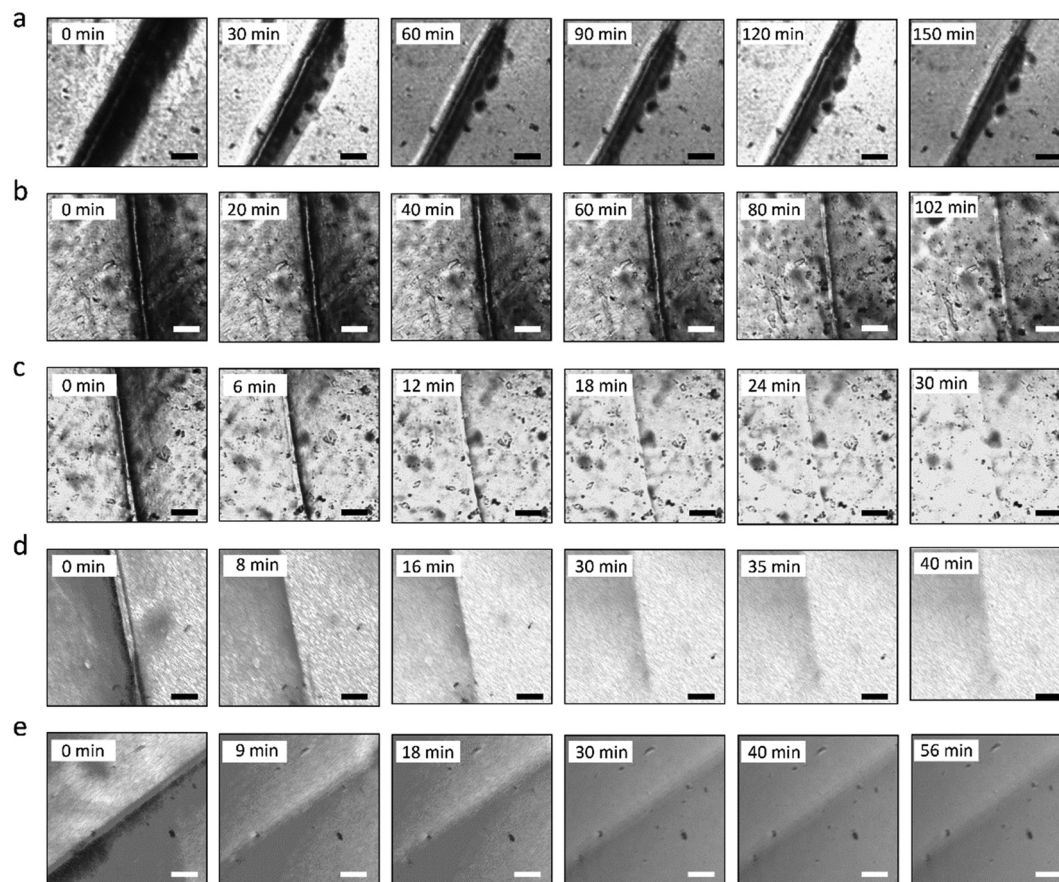
Fig. 6 Self-healing processes for the WPU–Ag@S series observed under an optical microscope: (a) WPU–Ag@S-0.00; (b) WPU–Ag@S-0.25; (c) WPU–Ag@S-0.50; (d) WPU–Ag@S-0.75; (e) WPU–Ag@S-1.00; scale bar: 30 μm.

these two factors, the self-healing time exhibited a decreasing and then increasing trend, reaching the smallest value for WPU–Ag@S-0.5. This phenomenon is closely related to the microstructure of WPU–Ag@S, as the Ag–thiolate interactions not only play the role of modifying the strength of the matrix but also facilitate dynamic exchange reactions to heal the microcrack.

Self-healing mechanics is the most straightforward method to characterize the self-healing property. Dumbbell-shaped specimens with microcracks were placed at room temperature for a period of time, and their mechanical properties were compared with those of samples without microcracks. The self-healing efficiency can be obtained using eqn (3) and (4):

$$\eta_\sigma = \frac{\sigma_s}{\sigma_o} \times 100\% \qquad (3)$$

$$\eta_\varepsilon = \frac{\varepsilon_s}{\varepsilon_o} \times 100\% \qquad (4)$$

where σ_s is the tensile strength of the self-healing samples, σ_o is the tensile strength of the original samples, η_σ is the self-healing efficiency for the tensile strength, ε_s is the elongation at break of the self-healing samples, ε_o is the elongation at break of the original samples, and η_ε is the self-healing efficiency for the elongation at break. Fig. 7 presents the self-healing mechanical curves for the WPU–Ag@S series at room temperature. As seen in

Fig. 7(a), the self-healing efficiency for the tensile strength exhibits an increasing and decreasing trend and reaches a maximum value of 98.69% for WPU–Ag@S-0.50. This is due to the self-healing performance compounding effects of the complex Ag NPs and flexible 3,6-dioxa-1,8-octanedithiol, endowing WPU–Ag@S-0.5 with the highest self-healing efficiency. Yang et al.[40–42] also obtained similar experimental results. The detailed self-healing mechanical property data with different contents of Ag–thiol coordination bonds are listed in Table S5 (ESI†). Fig. 7(b) shows the self-healing mechanical curves of WPU–Ag@S-0.5 for various times at room temperature. With an increase in the self-healing time, the tensile strength and elongation at break as well as the self-healing efficiency of WPU–Ag@S-0.50 increase. Particularly at 30 min, the self-healing efficiency approaches nearly 100%, demonstrating that this sample is an excellent room-temperature self-healing material. The detailed self-healing mechanical property data over time are listed in Table S6 (ESI†).

The rheology test results at 30 °C are shown in Fig. 8. There exists a cross point between the logarithm of the storage modulus and the loss modulus, defined as the critical angular frequency ω_c.[23] The reciprocal value of ω_c is the relaxation time τ, which is used to measure the rate of the dynamic reversible exchange reactions of the Ag–thiol coordination bonds. The data for ω_c and τ are shown in Table 3. When the Ag–thiol
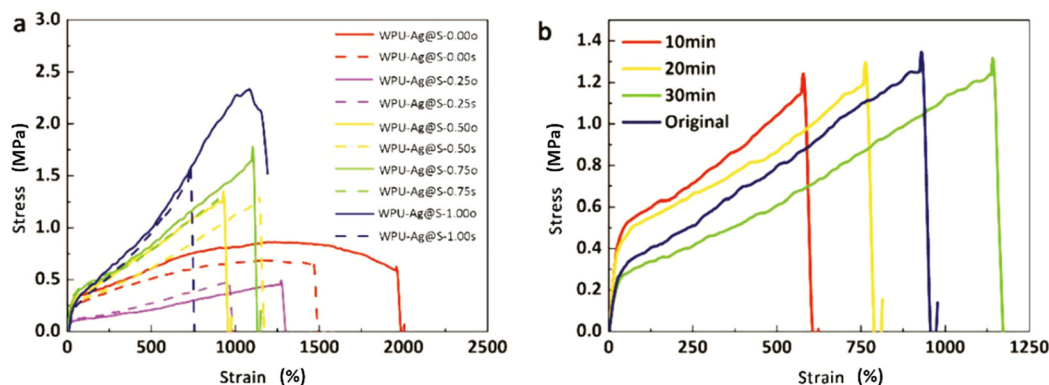
Fig. 7 (a) Self-healing mechanical performance of the original samples (solid lines) and the self-healing samples (dashed lines) for the WPU−Ag@S series. (b) Self-healing mechanical performance of WPU−Ag@S-0.50 at different self-healing times.

coordination bonds increase to the ratio of 0.50, ω_c reaches a maximum value of 2.179, which corresponds to the smallest relaxation time τ of 0.459 s. This result indicates that the rate of dynamic reversible exchange reactions for WPU−Ag@S-0.50 is the fastest due to suitable Ag–thiol coordination interactions and easy mobility of the WPU molecular chain. When the ratio of Ag–thiol coordination bonds increases to 1.00, the more dynamic reversible crosslinked points limit molecular chain movements and affect the exchange reactions of the Ag–thiol coordination bonds, causing the relaxation time τ to increase. All the rheological curves of WPU−Ag@S possess cross points, demonstrating that the Ag–thiol coordination bonds remain in the dynamic state at 30 °C.

Through optical microscopy, tensile mechanics, and rheology tests, the self-healing properties were observed, quantified, and confirmed. Here, we speculate that the self-healing mechanism

Table 3 Data of critical frequency ω_c and relaxation time τ for the WPU−Ag@S series

WPU−Ag@S	0.00	0.25	0.50	0.75	1.00
ω (rad s^{-1})	0.215	2.147	2.179	0.806	0.212
τ (s)	4.650	0.466	0.459	1.241	4.717

was greatly affected by the dynamic reversible exchange reactions of the Ag–thiol coordination bonds, as shown in Fig. 9. A little microcrack appears on the surface of the matrix (Fig. 9(a)). As the material matrix is relatively soft, it quickly experiences approaching movements or plastic flow at room temperature. Once the two faces of the microcrack are close enough, the Ag–thiol coordination bonds rearrange and associate with the neighboring Ag NPs, as shown in Fig. 9(b), resulting in dynamic
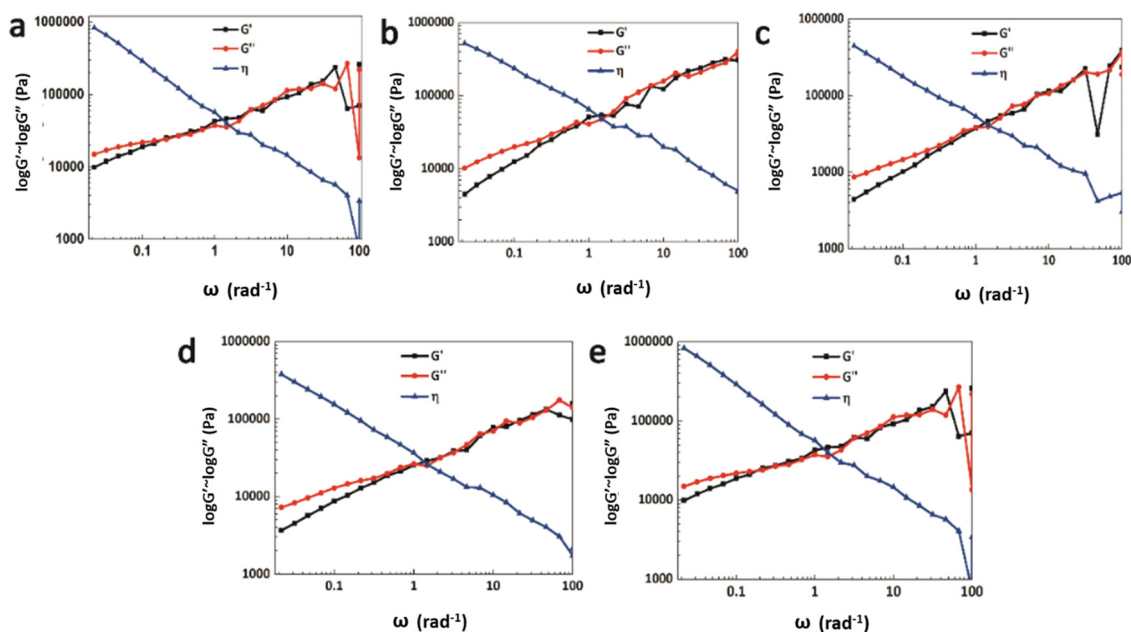

Fig. 8 Rheology test results for the WPU−Ag@S series: (a) WPU−Ag@S-0.00; (b) WPU−Ag@S-0.25; (c) WPU−Ag@S-0.50; (d) WPU−Ag@S-0.75 and (e) WPU−Ag@S-1.00.
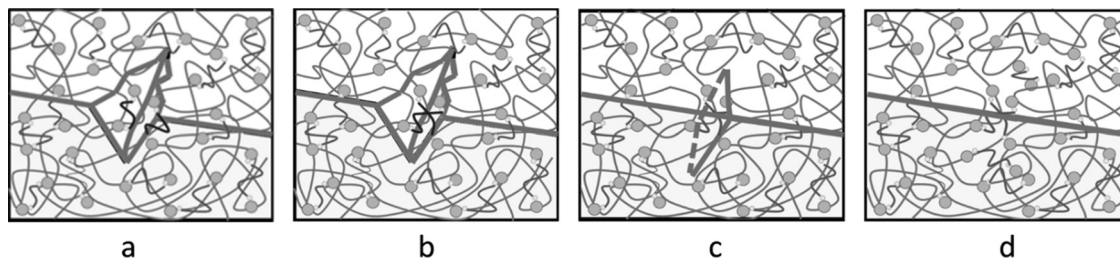
Fig. 9 Microscale self-healing mechanism for the WPU–Ag@S series: (a) microcrack approach, (b) dynamic exchange reactions of the −Ag@S− coordination bonds, (c) self-healing, and (d) recovery to the original state.

reversible exchange reactions[16] and the bonding of the two faces of the microcrack, as shown in Fig. 9(c). Finally, the microcrack disappears, and the material recovers to the original state, as shown in Fig. 9(d), achieving the target of self-healing.

4. Conclusions

In this work, Ag–thiol coordination bonds were introduced into the WPU matrix, forming a WPU–Ag@S elastomer with dynamic crosslinking networks, which showed excellent room-temperature self-healing properties. For the preparation of WPU–Ag, H_2O_2 was used to reduce Ag_2O NPs to Ag NPs. This method was quick and did not introduce any impurities in the WPU emulsions, making it a green and straightforward approach. After introducing the hydrophilic difunctional thiol into WPU–Ag, the formed WPU–Ag@S achieved self-healing at room temperature. Among the different samples of the WPU–Ag@S series, WPU–Ag@S-0.50 showed the shortest self-healing time and optimum self-healing efficiency. Therefore, it is a promising material for use as an environmentally friendly self-healing material.

Author contributions

Mengyun Zhang; Conceptualization, writing, review, and editing, Mengyun Zhang and Rimin Cong; methodology, formal analysis, and investigation, Shanjun Ding; Software, validation, and data curation, Yunjun Luo; resources, visualization, supervision, funding acquisition, and project administration, all the authors have read and agreed to the published version of the manuscript.

Conflicts of interest

The authors declare no conflict of interest.

Acknowledgements

References

1 S. R. White, N. R. Sottos, P. H. Geubelle, J. S. Moore, M. R. Kessler and S. Sriram, *et al.*, Autonomic healing of polymer composites, *Nature*, 2001, **409**(6822), 794–797.

2 Self-repairing, self-forming, and self-sensing systems for ceramic/polymer composites, in *Smart Structures and Materials 2002: Smart Structures and Integrated Systems*, ed. C. M. Dry, International Society for Optics and Photonics, 2002.

3 Passive smart self-repair in polymer matrix composite materials, in *Smart Structures and Materials 1993: Smart Materials*, ed. C. M. Dry and N. R. Sottos, International Society for Optics and Photonics, 1993.

4 K. S. Toohey, N. R. Sottos, J. A. Lewis, J. S. Moore and S. R. White, Self-healing materials with microvascular networks, *Nat. Mater.*, 2007, **6**(8), 581–585.

5 S. H. Söntjens, R. P. Sijbesma, M. H. van Genderen and E. Meijer, Stability and lifetime of quadruply hydrogen bonded 2-ureido-4 [1*H*]-pyrimidinone dimers, *J. Am. Chem. Soc.*, 2000, **122**(31), 7487–7493.

6 J. Canadell, H. Goossens and B. Klumperman, Self-healing materials based on disulfide links, *Macromolecules*, 2011, **44**(8), 2536–2541.

7 J. M. Matxain, J. M. Asua and F. Ruipérez, Design of new disulfide-based organic compounds for the improvement of self-healing materials, *Phys. Chem. Chem. Phys.*, 2016, **18**(3), 1758–1770.

8 A. Rekondo, R. Martin, A. Ruiz de Luzuriaga, G. Cabañero, H. J. Grande and I. Odriozola, Catalyst-free room-temperature self-healing elastomers based on aromatic disulfide metathesis, *Mater. Horiz.*, 2014, **1**(2), 237–240.

9 P. A. Pratama, M. Sharifi, A. M. Peterson and G. R. Palmese, Room Temperature Self-Healing Thermoset Based on the Diels–Alder Reaction, *ACS Appl. Mater. Interfaces*, 2013, **5**(23), 12425–12431.

10 P. K. Behera, S. K. Raut, P. Mondal, S. Sarkar and N. K. Singha, Self-Healable Polyurethane Elastomer Based on Dual Dynamic Covalent Chemistry Using Diels–Alder "Click" and Disulfide Metathesis Reactions, *ACS Appl. Polym. Mater.*, 2021, **3**(2), 847–856.

11 P. Du, X. Liu, Z. Zheng, X. Wang, T. Joncheray and Y. Zhang, Synthesis and characterization of linear self-healing polyurethane based on thermally reversible Diels–Alder reaction, *RSC Adv.*, 2013, **3**(35), 15475–15482.

12 J. S. Park, T. Darlington, A. F. Starr, K. Takahashi, J. Riendeau and H. Thomas Hahn, Multiple healing effect of thermally

activated self-healing composites based on Diels–Alder reaction, *Compos. Sci. Technol.*, 2010, **70**(15), 2154–2159.

13 G. Postiglione, S. Turri and M. Levi, Effect of the plasticizer on the self-healing properties of a polymer coating based on the thermoreversible Diels–Alder reaction, *Prog. Org. Coat.*, 2015, **78**, 526–531.

14 S. Zechel, M. D. Hager, T. Priemel and M. J. Harrington, Healing through histidine: Bioinspired pathways to self-healing polymers via imidazole–metal coordination, *Biomimetics.*, 2019, **4**(1), 20.

15 H. Qin, T. Zhang, H.-N. Li, H.-P. Cong, M. Antonietti and S.-H. Yu, Dynamic Au-Thiolate Interaction Induced Rapid Self-Healing Nanocomposite Hydrogels with Remarkable Mechanical Behaviors, *Chem.*, 2017, **3**(4), 691–705.

16 R. Martín, A. Rekondo, J. Echeberria, G. Cabañero, H. J. Grande and I. Odriozola, Room temperature self-healing power of silicone elastomers having silver nanoparticles as crosslinkers, *Chem. Commun.*, 2012, **48**(66), 8255–8257.

17 P. Song, H. Qin, H.-L. Gao, H.-P. Cong and S.-H. Yu, Self-healing and superstretchable conductors from hierarchical nanowire assemblies, *Nat. Commun.*, 2018, **9**(1), 2786.

18 H. Chen, R. Cheng, X. Zhao, Y. Zhang, A. Tam and Y. Yan, *et al.*, An injectable self-healing coordinative hydrogel with antibacterial and angiogenic properties for diabetic skin wound repair, *NPG Asia Mater.*, 2019, **11**(1), 3.

19 J. Xu, J. Chen, Y. Zhang, T. Liu and J. Fu, A Fast Room-Temperature Self-Healing Glassy Polyurethane, *Angew. Chem., Int. Ed.*, 2021, **60**(14), 7947–7955.

20 D. Montarnal, M. Capelot, F. Tournilhac and L. Leibler, Silica-like malleable materials from permanent organic networks, *Science*, 2011, **334**(6058), 965–968.

21 M. Capelot, D. Montarnal, F. Tournilhac and L. Leibler, Metal-catalyzed transesterification for healing and assembling of thermosets, *J. Am. Chem. Soc.*, 2012, **134**(18), 7664–7667.

22 S. Bokern, Z. Fan, C. Mattheis, A. Greiner and S. Agarwal, Synthesis of New Thermoplastic Elastomers by Silver Nanoparticles as Cross-Linker, *Macromolecules*, 2011, **44**(12), 5036–5042.

23 P. Casuso, I. Odriozola, A. Pérez-San Vicente, I. Loinaz, G. Cabañero and H.-Jr Grande, *et al.*, Injectable and self-healing dynamic hydrogels based on metal (I)-thiolate/disulfide exchange as biomaterials with tunable mechanical properties, *Biomacromolecules*, 2015, **16**(11), 3552–3561.

24 Y. Wattanodorn, R. Jenkan, P. Atorngitjawat and S. Wirasate, Antibacterial anionic waterborne polyurethanes/Ag nanocomposites with enhanced mechanical properties, *Polym. Test.*, 2014, **40**, 163–169.

25 M. G. Ventura, A. J. Parola and A. P. de Matos, Influence of heat treatment on the colour of Au and Ag glasses produced by the sol–gel pathway, *J. Non-Cryst. Solids*, 2011, **357**(4), 1342–1349.

26 N. Xiao, H. Liang and J. Lu, Degradable and biocompatible aldehyde-functionalized glycopolymer conjugated with doxorubicinvia acid-labile Schiff base linkage for pH-triggered drug release, *Soft Matter*, 2011, **7**(22), 10834–10840.

27 H. Nersisyan, J. Lee, H. Son, C. Won and D. Maeng, A new and effective chemical reduction method for preparation of nanosized silver powder and colloid dispersion, *Mater. Res. Bull.*, 2003, **38**(6), 949–956.

28 G. Liu, C. Xu, H. Chen, X. Hou and Y. Liu, Electroless deposition method for silver-coated carbon fibres, *Micro Nano Lett.*, 2015, **10**(6), 315–317.

29 J. Massera, A. Martin, J. Choi, T. Anderson, L. Petit and M. Richardson, *et al.*, Spatially controlled dissolution of Ag nanoparticles in irradiated SiO2 sol–gel film, *J. Phys. Chem. Solids*, 2010, **71**(12), 1634–1638.

30 B. Mahltig, E. Gutmann, M. Reibold, D. C. Meyer and H. Böttcher, Synthesis of Ag and Ag/SiO2 sols by solvothermal method and their bactericidal activity, *J. Sol-Gel Sci. Technol.*, 2009, **51**(2), 204–214.

31 D. Macocinschi, D. Filip, M. F. Zaltariov and C. D. Varganici, Thermal and hydrolytic stability of silver nanoparticle polyurethane biocomposites for medical applications, *Polym. Degrad. Stab.*, 2015, **121**, 238–246.

32 H. Deka, N. Karak, R. D. Kalita and A. K. Buragohain, Bio-based thermostable, biodegradable and biocompatible hyperbranched polyurethane/Ag nanocomposites with antimicrobial activity, *Polym. Degrad. Stab.*, 2010, **95**(9), 1509–1517.

33 R. Qu, J. Gao, B. Tang, Q. Ma, B. Qu and C. Sun, Preparation and property of polyurethane/nanosilver complex fibers, *Appl. Surf. Sci.*, 2014, **294**, 81–88.

34 X. Zhang, M. Zhu, W. Wang and D. Yu, Silver/waterborne polyurethane-acrylate's antibacterial coating on cotton fabric based on click reaction via ultraviolet radiation, *Prog. Org. Coat.*, 2018, **120**, 10–18.

35 M. Liu, C. Zhang, W. W. Tjiu, Z. Yang, W. Wang and T. Liu, One-step hybridization of graphene nanoribbons with carbon nanotubes and its strong-yet-ductile thermoplastic polyurethane composites, *Polymer*, 2013, **54**(12), 3124–3130.

36 M. Zhang, F. Zhao and Y. Luo, Self-Healing Mechanism of Microcracks on Waterborne Polyurethane with Tunable Disulfide Bond Contents, *ACS Omega*, 2019, **4**(1), 1703–1714.

37 A. Mohammadi, A. H. Doctorsafaei, S. B. Burujeny, H. A. Rudbari, N. Kordestani and S. A. A. Najafabadi, Silver (I) complex with a Schiff base ligand extended waterborne polyurethane: A developed strategy to obtain a highly stable antibacterial dispersion impregnated with in situ formed silver nanoparticles, *Chem. Eng. J.*, 2020, **381**, 122776.

38 L. Lei, L. Zhong, X. Lin, Y. Li and Z. Xia, Synthesis and characterization of waterborne polyurethane dispersions with different chain extenders for potential application in waterborne ink, *Chem. Eng. J.*, 2014, **253**, 518–525.

39 G. Trovati, E. A. Sanches, S. C. Neto, Y. P. Mascarenhas and G. O. Chierice, Characterization of polyurethane resins by FTIR, TGA, and XRD, *J. Appl. Polym. Sci.*, 2010, **115**(1), 263–268.

40 S. Xu, D. Sheng, X. Liu, F. Ji, Y. Zhou and L. Dong, *et al.*, A seawater-assisted self-healing metal–catechol polyurethane with tunable mechanical properties, *Polym. Int.*, 2019, **68**(6), 1084–1090.

41 S. Xu, D. Sheng, Y. Zhou, H. Wu, H. Xie and X. Tian, *et al.*, A dual supramolecular crosslinked polyurethane with superior mechanical properties and autonomous self-healing ability, *New J. Chem.*, 2020, **44**(18), 7395–7400.

42 S. Xu, D. Sheng, Y. Zhou, H. Wu, H. Xie and X. Liu, *et al.*, A robust and healable polyurethane based on coordination bonds, *Polym. Int.*, 2020, **69**(9), 876–882.